

# Process, design rule, and layout co-optimization for DSA based patterning of sub-10nm Finfet devices

Joydeep Mitra<sup>1</sup>, Andres Torres<sup>1</sup>, and David Z Pan<sup>2</sup>

<sup>1</sup>Mentor Graphics Corporation

<sup>2</sup>University of Texas at Austin

## ABSTRACT

As we reach the limits of current patterning techniques led by 193nm immersion lithography, the focus is on next generation patterning techniques such as Extreme Ultra Violet Lithography (EUVL) and Directed Self Assembly (DSA) to enable 7nm and 5nm technology nodes. Though there have been great strides in materials development for DSA with high  $\chi$  materials enabling up to 5 nm pitches, DSA still lacks the EDA tool support to enable adoption in layout design and high volume manufacturing. In this paper we plan to alleviate this gap by proposing a framework that encompasses the problems of DSA-aware layout decomposition, grouping and compliance, Guiding Pattern (GP) synthesis, RET and final verification. The above framework will also enumerate the variations of each of the above steps for DSA candidate layers such as vias, fins and metal lines. As components of the above framework, we first propose a family of practical full-chip hybrid multi-patterning(MP)/DSA-aware decomposition algorithms capable of using DSA as a relaxation method for reducing coloring conflicts. We then propose a model based GP synthesis algorithm for generating GPs with arbitrary via topologies capable of accurate via placement and also resilient to via phase transition during assembly. The vias assembled using these GPs also show resilience towards post RET process variations. We then perform a Monte-Carlo simulation based feasibility analysis applying DSA to printing of Finfets which shows the pros and cons of using DSA over Self-aligned Double Patterning (SADP) which is the existing technology for printing Fins. We also introduce layout decomposition algorithms for DSA GP and optical trim mask co-optimization.

## 1. INTRODUCTION

Among the available MPL techniques, Self-Aligned Double Patterning (SADP) remains the preferred technology for the finest-pitch CD device layers such as the fin layer.<sup>3</sup> FinFet devices are currently receiving a lot of attention at advanced technology nodes since the FinFet device architecture enables scaling by increasing fin density within the active area<sup>1,2</sup> thus achieving increased effective device widths. It is this increasing fin density that has left SADP as the only viable patterning technique for printing fins.<sup>3</sup> SADP consists of two patterning steps for fins; 1) a Mandrel mask for spacer deposition, etch back and fin deposition and 2) a trim mask for etching away unwanted structures such as dummy Mandrel.

Hence the SADP technique imposes additional design constraints for the fin structures where extra space needs to be allocated for dummy Mandrel in the case of an odd number of fins. This in turn requires more aggressive resolution enhancement techniques (RET) for the trim mask. The motivation of this section is to analyze DSA as an alternative patterning technique to SADP for fins, since DSA can assemble any arbitrary number of lamellar structures within the confines of a Grapho-epitaxy based guiding pattern trench,<sup>7</sup> thus alleviating the previously mentioned design constraint imposed by SADP as depicted in fig.1.

In order to achieve the pattern fidelity required by the original drawn target, it is necessary to obtain a set of guiding patterns that will achieve the assembly of the desired fin patterns. The challenge for using DSA today to assemble the desired fin structures while taking advantage of density multiplication within a guiding pattern is that if the provided guiding patterns are not commensurable to the natural period of the diblock copolymer, random structures may assemble as shown in fig.2(b) below. Fig.2(a) shows a group of four conformal fins assembled inside a larger guiding pattern, where the left and right bridges will later be trimmed away. What is needed is a systematic process flow that will co-optimize two objectives: 1) generate guiding patterns that will achieve a fin assembly which will maximize fidelity towards the drawn target and 2) generate a trim mask which will minimize the RET effort needed.

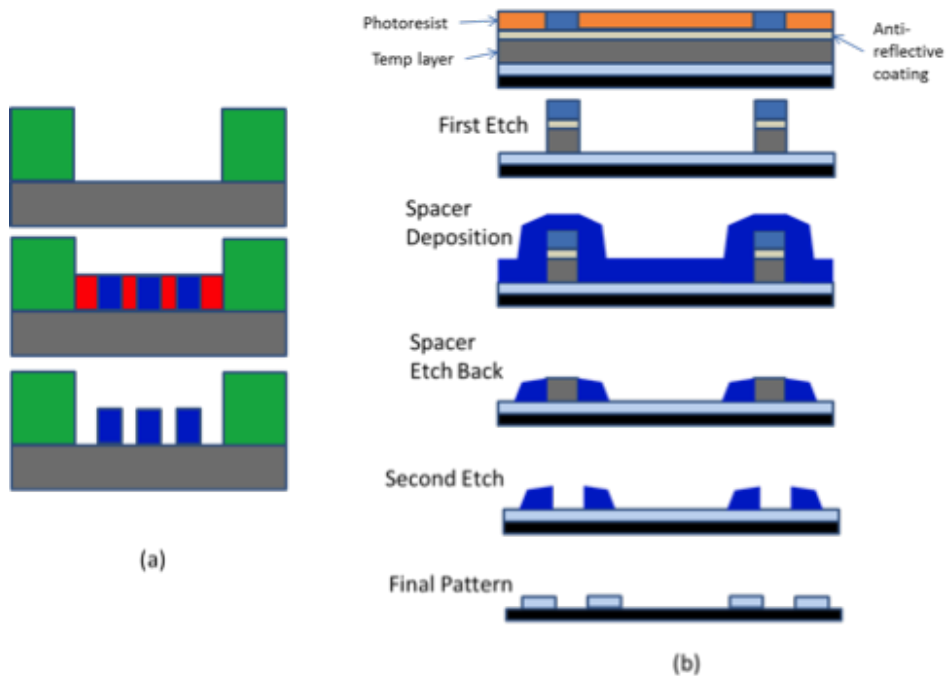


Figure 1. (a) DSA process steps which shows 1.) An initial exposure and etch step for the grapho-epitaxial guiding pattern trench; 2.) Block co-polymer deposition and assembly and 3.) Removal of one co-polymer component; (b) SADP process steps illustrating the formation of an even parity of fins, some of which may need to be trimmed away if an odd number of fins is required.

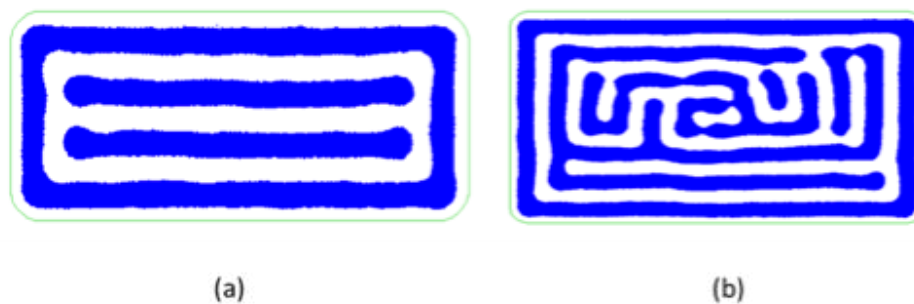


Figure 2. (a) A group of 4 fins assembled inside a single guiding pattern before trimming. (b) Non-conformal guiding pattern.

The key contributions of this paper are as follows:

- A first patterning methodology leveraging the pitch multiplication property of DSA in manufacturing the fin layer with comparable or better fidelity than SADP but without the even parity constraint of SADP.
- A first simulation based study and systematic organization of DSA guiding pattern shapes and aspect ratios to optimize the printability of fins. This study also optimized the chemical composition of the DSA process to best target a given fin pitch and CD.
- A first layout decomposition algorithm for fins using the DSA process based on guidelines obtained from 2 above which partitions fin clusters into optimal groups and then decomposes the resulting groups into guiding pattern and trim masks.

The remainder of this paper is organized into the following sections. In section 2 we will formulate the desired objectives and describe our experimental setup and the overall simulation data flow. In section 3 we will analyze

the simulation results and extract the ranges of conformal guiding patterns. In section 4 we will describe a layout decomposition algorithm that will apply the conformal guiding patterns from section 3 into optimal fin groups and trim mask. In section 5 we will apply the above algorithm to several layout scenarios and analyze the results. We will finally conclude in section 6.

## 2. EXPERIMENTAL SETUP AND SIMULATION DATA FLOW

The process of self-assembly of regular lamellar and cylindrical patterns through phase segregation of two molecular species such as Polystyrene (PS) and Polymethyl methacrylate (PMMA) has been extensively studied.<sup>8,11</sup> The extent to which the two species segregate and the types of patterns formed (lamellar, cylindrical, spherical or others) are determined by the molecular weight and ratio of each of the species within the diblock copolymer. The phase formation into structural orientations can be guided through various mechanisms. Our simulations will be based on the most widely used of these guiding processes namely Grapho-epitaxy<sup>5,6,9</sup> which is essentially a guiding trench that enables the walls of the guiding pattern to provide a configuration axis of alignment for the polymer. A Monte-Carlo molecular simulator<sup>4</sup> was used as the core engine to generate the final fin contours based upon guiding patterns which were provided to the simulator as an input. We chose a Monte Carlo approach over self-consistent field theory methods (SCFT) since Monte Carlo simulations are able to capture the thermal fluctuations that give rise to proper assembly, thus allowing exploration of more feasible configurations. The simulation and analysis system is depicted in fig.3 and is described in detail later in this section.

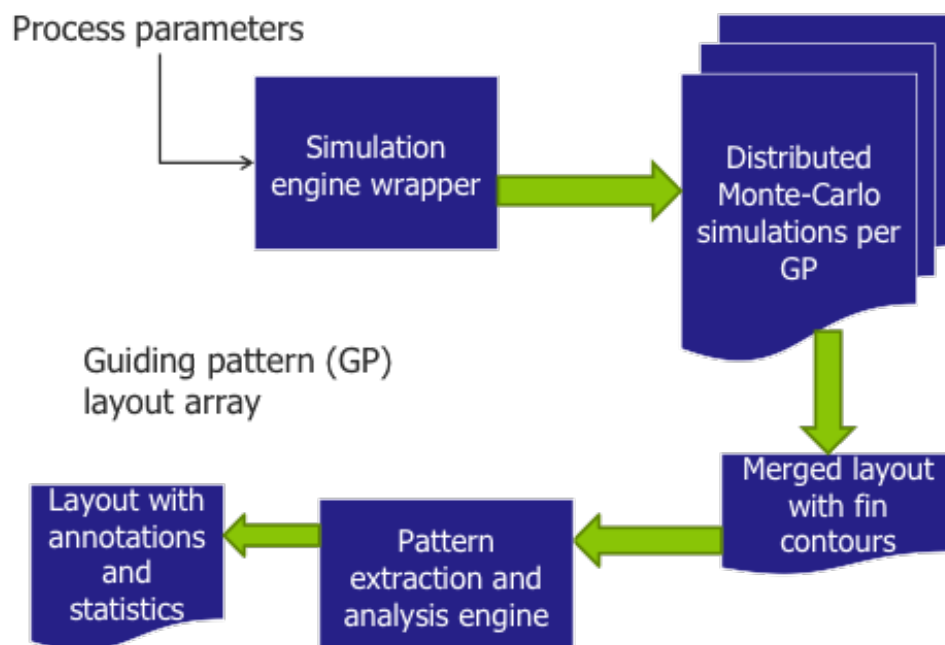


Figure 3. Simulation and Analysis Flow.

Some of the process parameters provided to the system included:

1. The volume fraction of diblock copolymer compared to homopolymer.
2. Volume fraction of homopolymers.
3. Diblock composition.
4. A class of parameters including chain density and compressibility, all of which are functions of the molecular weight of the block copolymer.

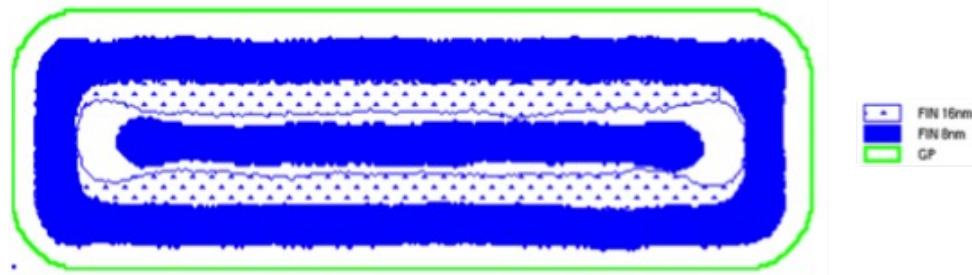


Figure 4. Higher and lower fin densities (pitch of 36nm and 48nm) assembled by using lower and higher molecular weights (55 and 75) respectively.

We maintained an equal ratio between the two polymers in the diblock copolymer. We introduced small quantities of homopolymer (2% and 5%) to see if the reduced amount of each polymer species would cause less fracturing and more alignment, our conclusion was that homopolymer actually hindered the alignment process and we settled on 100% diblock copolymer. We achieved the required pitch and CD of the fins for the given 7nm technology node (fin pitch of 36nm) by varying the molecular weight and hence the class of parameters in item 4 above. The lower the molecular weight, the tighter will be the pitch and device width. Fig. 4 shows 2 and 3 fins forming within the same guiding pattern of width 90nm using block copolymer molecular weights of 75 and 55 respectively. We initially started with 25K moves, but finally settled on 75K moves, since the potential energy per bond per molecule was not reaching equilibrium with the lower number of moves. This is depicted in fig.5.

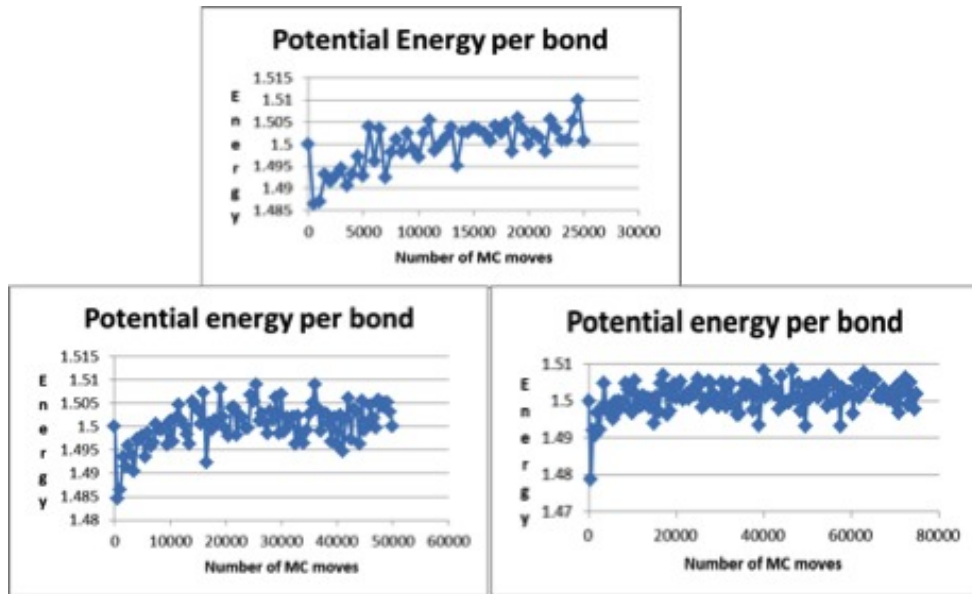


Figure 5. 75K Monte-Carlo moves for energy equilibrium.

Our system as depicted in fig.3 consisted of a simulation wrapper which accepted an Oasis layout<sup>10</sup> containing an array of guiding patterns as input and generated distributed simulation jobs with each job consisting of a single guiding pattern of a specific aspect ratio running concurrently on separate machines. We began with some corner simulations and finally settled on an exploration range of aspect ratios with the guiding pattern length varying from 250nm to 550nm and the height varying from 25nm to 320nm in steps of 5nm.

Fig.6 shows two typical guiding pattern simulations, the first conforming at 180nm trimmed length (14nm fin width to be plasma etched down to 8nm) and the second non-conformal. Once all the simulations had completed, the simulation output was first converted into fin layout contours and finally all the layouts were merged into one composite layout. The composite layout was then merged with another layout consisting of the trim mask.

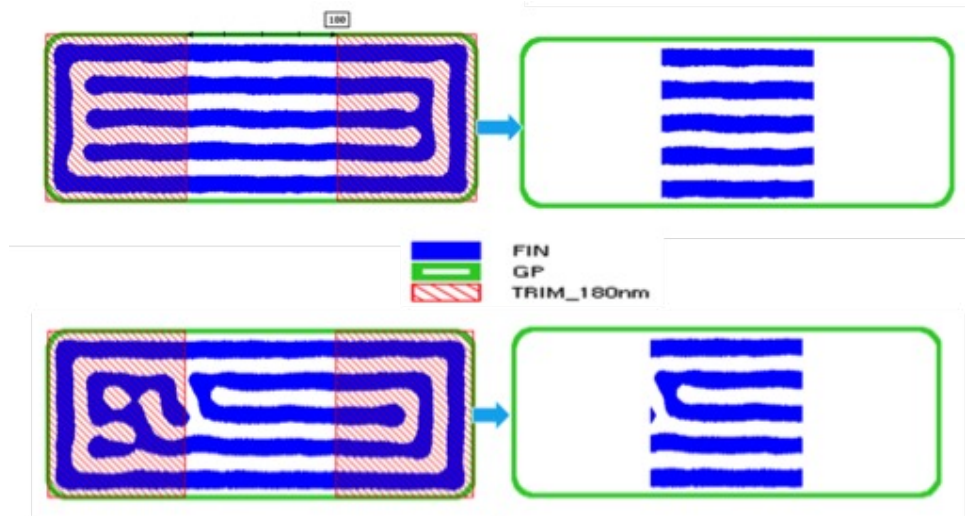


Figure 6. The trim mask (red) and the guiding pattern (green) have been sized to extract a group of 5 fins of length 180nm. The top two layouts are conformal, unlike the bottom two.

This composite layout was then fed to the Calibre DRC/DFM polygon engine<sup>10</sup> along with an analysis rule deck to filter out non-conformal layouts. The final annotated layout could then be viewed and analyzed using the Calibre rule verification engine (RVE).<sup>10</sup>

Our ultimate objectives for the above simulation system are twofold:

1. Is there a pattern of friendly guiding patterns that can then be formulated into a mask synthesis objective function for generating a mask for guiding patterns and
2. assuming that we do find a pattern of friendly guiding patterns, can we then formulate another mask synthesis objective function for the trim mask to minimize the effort of the RET required for the trim mask?

### 3. ANALYSIS OF SIMULATION RESULTS

#### 3.1 Fixed extracted fin length

Since our composite layout of fins and guiding patterns consisted of a 60X60 grid of rectangular guiding patterns (GP) with varying aspect ratio, we will first restrict our analysis to a single extracted fin length and then expand the analysis to variable fin lengths in section 3.2. Fig.7 depicts a color mapping of our GP grid into clusters of GPs containing 1 through 8 fins each with length 180nm (width 14nm to be plasma etched down to 8nm).

As can be observed, the grid of guiding patterns can now be classified into bands of conformal groups of fins each band consisting of GPs with a specific number of conformal fins after trimming the left and right edges by an amount to leave a core of length 180nm. The non colored regions correspond to forbidden regions of non conformal fins. It can be observed that the conformal regions are skewed towards the right with robust bands between 1 and 5 fin groups. The reason for this skew is explored and explained in section 3.2

#### 3.2 Multiple extracted fin lengths

We then ran the above analysis on a series of extracted fin lengths varying between 180nm and 360nm. Fig.8 depicts the results in a series of graphs. The X and Y axes correspond to the aspect ratio of the GP with the number of assembled fins within a GP of a specific aspect ratio being plotted on the Z axis. For each analysis run of a specific fin length, the trim masks were adjusted accordingly to only trim off the left and right edges of the fin contours to leave behind a core with the given fin length.



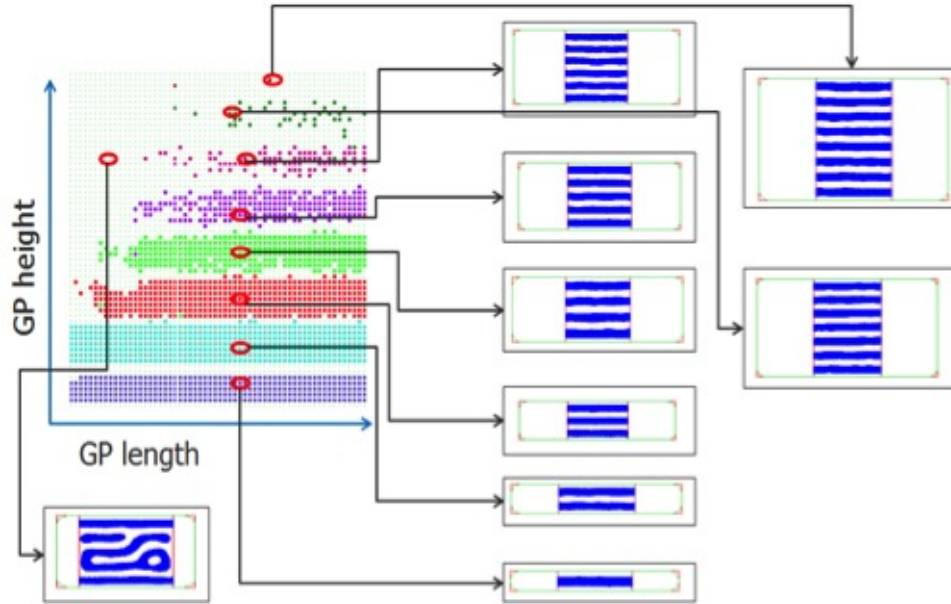


Figure 7. Composite layout with a grid of GPs of varying aspect ratios. Each point corresponds to a specific GP containing a set of assembled fins. The color map corresponds to the number of conformal fins within the GP.

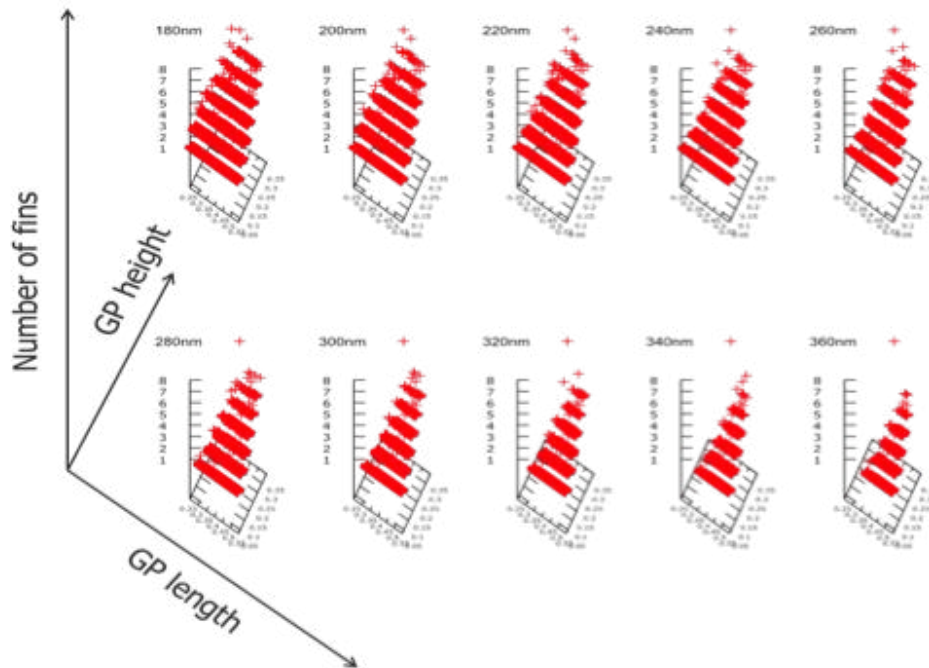


Figure 8. Each 3D plot above corresponds to a specific trimmed fin length (180nm - 360nm). The GP length and height correspond to the X and Y axes resp. and the number of fins is on the Z axis.

We note several observations from the above graphs in fig.8. Firstly, as expected, as we increase the required fin lengths we see a decrease in the bands of conformal fins in every group of GPs with specific numbers of fins. Secondly, we see that for all bands of conformal fins, the minimum GP length required for these fins is increasing. Finally we see that bands with a higher number of fins (6 through 8) become non-existent as we increase the required conformal fin length. All of the above observations can be explained by the fact that since we would like the horizontal (length) axis to be the preferred axis of orientation of the assembled fins, as we increase the

height of the GP, the vertical walls of the GP trench will also begin to influence the lamellar formations allowing additional degrees of freedom during phase segregation of the two species of polymer.

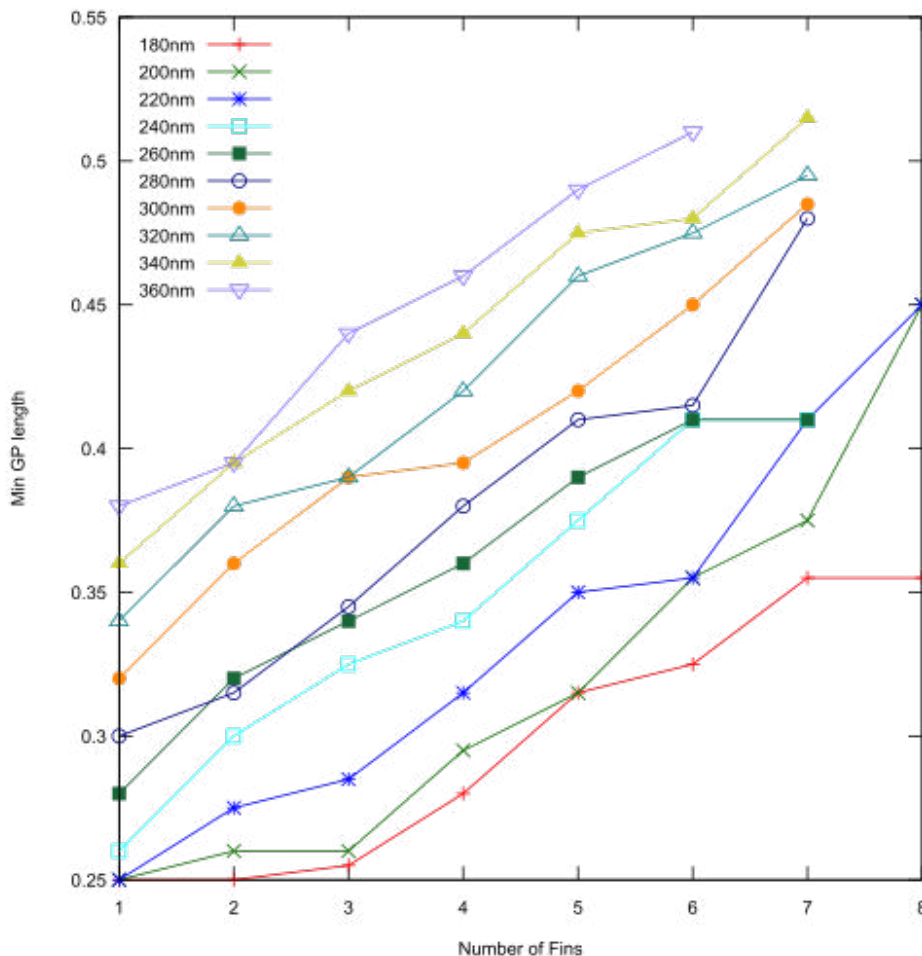


Figure 9. A plot of the minimum GP length required for assembling a specific number of conformal fins within the GP. Each colored plot corresponds to a specific trimmed fin length.

The above observations are captured on the graph in fig. 9. This graph will now form the basis of a critical layout decomposition mapping rule. From fig. 9 we see that as the required fin length increases, the corresponding minimum GP length also increases. We also see that the minimum GP length also increases as the number of fins per GP increases. Within a given circuit, FinFets are either multi-fingered or stacked devices,<sup>1</sup> hence the corresponding groups of fins are usually track aligned, fixed pitch groups of equal sized fins sharing the same active area. The lengths of fins may vary between active area to active area but within the same active area they are of fixed length and pitch. Hence, it will now be possible to read off or interpolate the desired GP aspect ratio from a table, given the required number of fins and the fin length. This will form the basis of section 4.

## 4. LAYOUT DECOMPOSITION INTO GP MASK AND TRIM MASK

### 4.1 Ideal Scenario: Isolated GPs

Based on our analysis in Section 3, we are now in a position to apply our study of conformal GPs to fin layout decomposition. Let us first consider the ideal scenario of multiple fin clusters in isolation with each cluster quite far from a neighboring cluster as depicted in fig. 10. With a 2D lookup table indexed by the number of fins

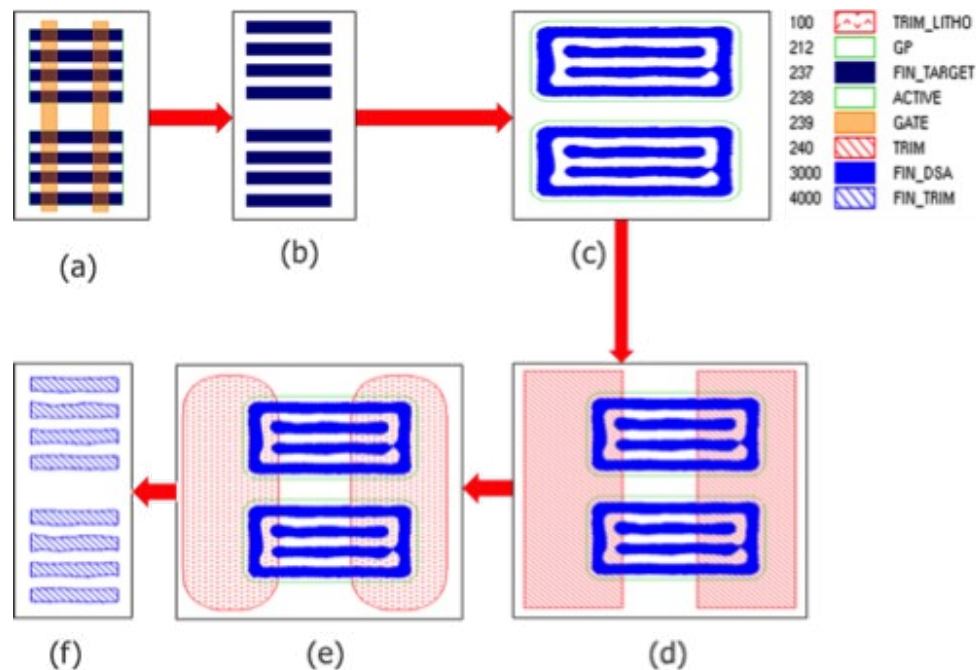


Figure 10. (a) Original drawn layout. (b) Original drawn fin targets only. (c) Group each fin cluster into conformal GPs and assemble fins. (d) Apply drawn trim mask. (e) Coarse aerial image of trim mask. (f) Final trimmed fins.

and the fin length, we can look up the appropriate minimum aspect ratio of the GP to achieve conformal fin assembly.

In the above ideal scenario, we have the fin clusters originally separated by a distance (say  $D$ ) which is greater than another distance (say  $L$ ) where  $L$  is the lithographic separation below which the GPs would have lithographic interference between each other such as bridging. Given the GP placements, the target trim mask is generated in such a way that the extracted trim length is no larger than the fin length index of the corresponding GP. Fig. 10(e) demonstrates the fact that since the lithographic coarse aerial image of the trim mask may not exactly match the original drawn trim mask, there is the potential of causing undesirable fin trimming. This ideal scenario avoids the incomplete trimming situation though this problem will be in effect in the next scenario that we will consider. We finally obtain the desired trimmed fins in fig. 10(f). The trim mask has the overlap flexibility such that it can be asymmetric as long as the extracted fin is smaller in length than the fin length index for the chosen GP. In other words, since smaller conformal fin lengths are contained within larger lengths, our trim mask has the flexibility of dimension between the larger and smaller trim lengths as depicted in fig. 11.

## 4.2 Merged GPs

Without explicit DSA design rules, it may be that clusters cannot be completely isolated from each other due to the need for tightly packed devices in standard cells, and there may be fin clusters within active areas which may be close enough such that the distance  $D$  may now be less than  $L$ . In this situation GPs need to be merged and the trim mask modified to achieve the desired target fins. In this scenario, we will have to look up from our 2D table a GP with an aspect ratio that can encapsulate a fin whose length is the largest of the concatenation of all fins within the merged GP, assuming that all fins are track aligned. The index for the number of fins in our 2D table corresponds to the number of fins in the largest fin cluster inside the merged GP.

Fig. 12 depicts a scenario where the fin clusters in fig. 10 have been brought closer together in the horizontal direction. Notice in this case figs. 12(d),(e) and (f) show that additional effort is needed from the trim mask due to the merging of the previous four guiding patterns into two due to the relative closeness of the fin clusters. The trim effort essentially translates to additional concave corners being introduced which leads to additional



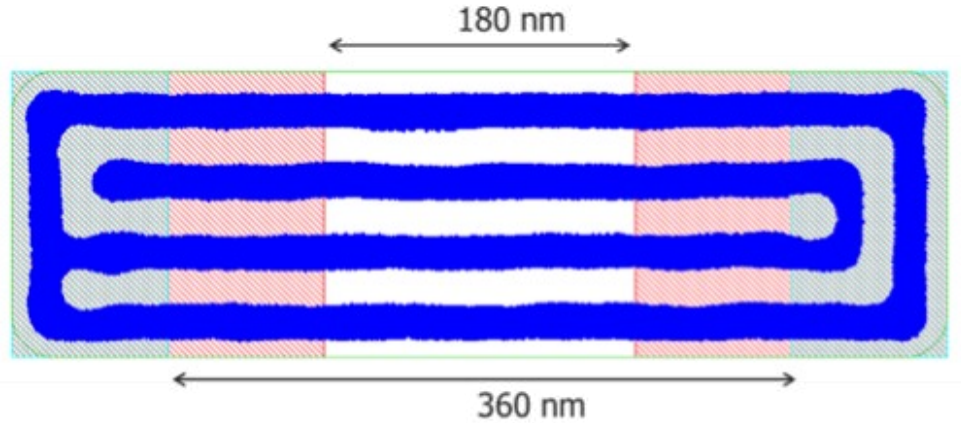


Figure 11. If a GP has been accepted as conformal with a larger length index (eg. 360 nm) it is implied that the GP is also conformal for smaller fin lengths. Hence the trim mask above has flexibility of dimension to include fin lengths of 360 nm and below.

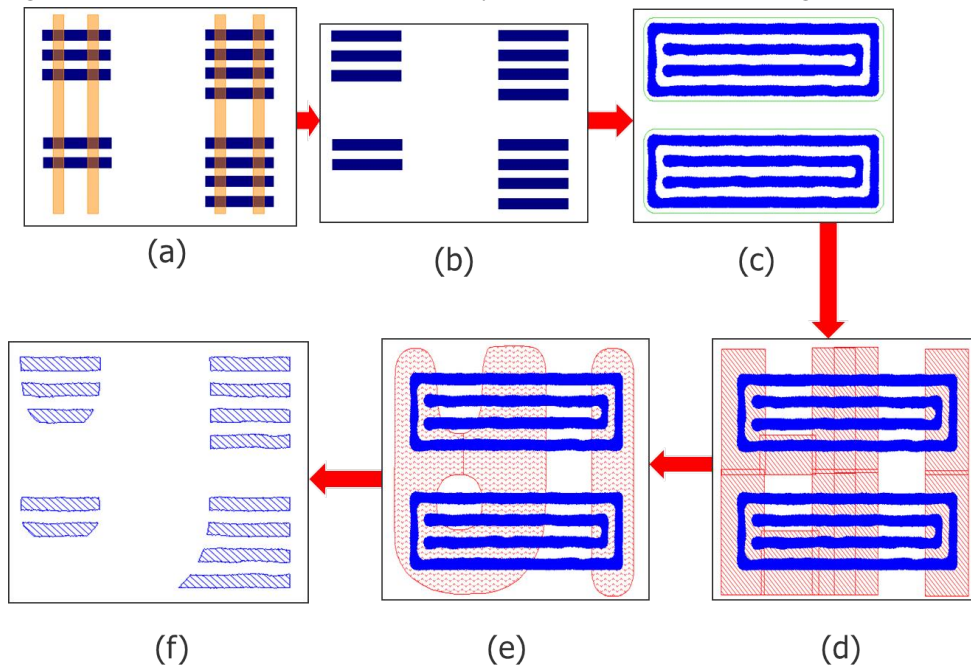


Figure 12. (a) Original drawn layout. (b) Original drawn fin targets only. (c) Merged GPs and fin assembly due to smaller inter-cluster distance. (d) Introduction of complex trim mask with additional concave corners. (e) Coarse aerial image of complex trim mask. (f) Final trimmed fins with undesirable asymmetric line ends.

trim curvatures intersecting with the fin contours. This ultimately causes asymmetric line ends which may in turn lead to unreliable overlap between fins and S/D pads.

### 4.3 Design Considerations

Hence we now propose two critical design guidelines as follows to achieve the best GPs with the least trim effort:

1. Increase the inter-cluster distance to be greater than  $L+T$  where  $T$  is an additional clearance between the fin line ends and the GP.
2. Maximize the placement of aligned fin clusters to have a matching number of fins wherever possible. Following the above guidelines will achieve a robust trim mask with a reduced number of concave corners in the vicinity of fin clusters.

## 4.4 Layout Decomposition

We are now in a position to formulate two layout decomposition algorithms, one for generating the guiding patterns and one for generating the trim mask.

---

**Algorithm 1** generate GP

---

**Require:** Track aligned fin layout clusters  $C$

**Ensure:** Conformal GPs covering all fins.

```
1: for each  $C_i$  in  $C$  do
2:    $M = MERGE C_i$ 
3: end for
4: for each isolated fin group  $m_j$  in  $M$  do
5:   for each track  $t_k$  inside  $m_j$  do
6:      $l_k =$  distance between extremal fin endpoints inside  $t_k$ 
7:   end for
8:    $l_j = max([l_k])$ 
9:    $n_j =$  number of fins in largest original cluster in  $m_j$ 
10:   $GP_j = GP[l_j][n_j]$ 
11: end for
```

---

---

**Algorithm 2** generate TRIM

---

**Require:** Guiding patterns  $GP$  generated by 1

**Ensure:** Trim masks encompassing non-required fin shapes.

```
1: for each guiding pattern  $g_i$  in  $GP$  do
2:    $l_i =$  core fin length inside  $g_i$ 
3:    $t_i =$  a pair of rectangles at the edges of  $g_i$  to leave core length  $l_i$  exposed.
4:    $T = ACCUMULATE t_i$ 
5: end for
6: for each  $t_i$  in  $T$  do
7:   MERGE  $t_i$  with neighbors closer than litho distance  $L$ 
8: end for
```

---

For each of the algorithms 1 and 2, the MERGE operation is essentially a Boolean OR of objects closer than the lithographic interaction distance  $L$ . In the case of 1, this is the distance between two neighboring GPs whereas in algorithm 2 it is the corresponding distance between two neighboring trim rectangles. It is to be noted that in algorithm 1, the 2D lookup data structure for GPs has the advantage of handling continuous fin lengths by virtue of the property demonstrated in fig. 11, section 4. If the required length  $l_j$  lies between two stored lengths such that  $l_j' \leq l_j \leq l_j''$  then we choose the GP corresponding to the larger length  $l_j''$  since we are guaranteed to maintain conformity even if we trim down to length  $l_j$ .

## 5. LAYOUT DECOMPOSITION RESULTS

We ran the above algorithms on a suite of benchmark circuits. In order to analyze the quality of results, we define three metrics:

1. the ratio of the number of skewed fins due to erroneous trimming, to the total number of fins
2. the ratio of the number of concave corners to the total number of corners, and
3. the ratio of the number of GPs containing a single fin cluster to the total number of GPs.

Table 1 depicts the results. We can see that there is a direct correlation between these metrics. As the number of single fin clusters increases, there is a decrease in both concave corners which will affect OPC masks

and a decrease in the number of poorly formed fins which is what we would expect. In other words, the more we isolate individual fin clusters, the less the trim effort required and hence the more fidelity we have of the trimmed fins to the original drawn target.

Table 1. Trim effort, fin quality based on ratio of isolated GPs

Circuit	$(Single\ fin\ GP)/(All\ GPs)$	$(Concave)/(All\ corners)$	$(Skewed\ fins)/(All\ fins)$
Circuit 1	0.31	0.59	0.35
Circuit 2	0.42	0.54	0.28
Circuit 3	0.47	0.54	0.27
Circuit 4	0.51	0.48	0.23
Circuit 5	0.59	0.42	0.19
Circuit 6	0.63	0.21	0.18
Circuit 7	0.67	0.2	0.18
Circuit 8	0.72	0.2	0.09
Circuit 9	0.73	0.14	0.07
Circuit 10	0.86	0.12	0.06
Circuit 11	0.55	0.44	0.19

## 6. CONCLUSION

In this paper, we introduced the first exhaustive simulation driven study of guiding patterns (GPs) for assembling fins using DSA where one of the simulation layout parameters was the aspect ratio of the GPs. We found that there was a pattern of horizontal feasible regions of GPs with robust formation of fins varying from 1 to 5 per GP. We extracted this data into a 2D lookup table of GPs indexed by the number of fins and fin length. This table also provided us trimming information because the useful fin length index corresponds to the robust fin length at the core of the GP allowing us to apply a symmetric trim mask on the edges perpendicular to the fin direction away from the core. We then provided design guidelines to reduce trimming effort and then formulated a fin layout decomposition algorithm for DSA. We finally applied our decomposition algorithm to a suite of circuits and enumerated three metrics to measure the adherence to the proposed design guidelines, the trim effort and the fidelity of the pattern formation to the original target.

We would like to reiterate that the patterning methodology outlined in this paper bounds the number of lithography steps to just two, the GP mask and the trim mask. The actual fin density multiplication is achieved by the process of DSA. As the process node shrinks, the prevailing patterning scheme of SADP can no longer be contained within two patterning steps but is headed towards more complex patterning technologies such as SAQP. In addition to an increase in cost, SAQP will also add complexity to the trimming process as well, in addition to the existing complexity of having to trim away dummy mandrel for an odd number of fins.

## REFERENCES

1. M. Alioto. Comparative evaluation of layout density in 3t, 4t, and mt finfet standard cells. *IEEE Transactions on VLSI Systems*, 19(5), 2011.
2. K. Anil et al. Layout density analysis of finfets. In *Solid-State Device Research European Conference*, 2003.
3. Degroote, R. Rooyackers, et al. Spacer defined finfet: Active area patterning of sub-20 nm fins with high density. *Journal of Microelectronic Engineering*, 84(4), 2007.
4. F. A. Detchevry, H. Kang, K. C. Daoulas, M. Muller, P. F. Nealey, and J. J. de Pablo. Monte carlo simulations of a coarse grain model for block copolymers and nanocomposites. *Macromolecules*, 41(13):4909–5001, 2008.
5. G. Fenger, A. Burbine, J. A. Torres, Y. Ma, Y. Granik, P. Krasnova, G. Vandenberghe, R. Gronheid, and J. Bekaert. Calibration and application of a dsa compact model for graphoepitaxy hole processes using contour-based metrology. In *Proc. SPIE 9235, Photomask Technology 2014, 92351X (8 October)*, 2014.

6. G. Fenger et al. Compact model experimental validation for grapho-epitaxy hole processes and its impact in mask making tolerances. In *Proceedings of SPIE 9231, 30th European Mask and Lithography Conference, October 17, 2014*.
7. R. Gronheid, Delgadillo, et al. Frequency multiplication of lamellar phase block copolymers with grapho-epitaxy directed self-assembly sensitivity to prepattern. *J. Micro/Nanolith. MEMS MOEMS.*, 0301303, 2012.
8. C.-C. Liu et al. Chemical patterns for directed self-assembly of lamellae-forming block copolymers with density multiplication of features. *macromolecules. Macromolecules*, 46(4), 2013.
9. Y. Ma, J. Torres, G. Fenger, Y. Granik, J. Ryckaert, G. Vanderberghe, J. Bekaert, and J. Word. Challenges and opportunities in applying grapho-epitaxy dsa lithography to metal cut and contact/via applications. In *30th European Mask and Lithography Conference, International Society for Optics and Photonics, 2014*, 2014.
10. Mentor Graphics Corp. *Calibre Workbench suite of tools*.
11. J. A. Torres et al. Physical verification and manufacturing of contact/via layers using grapho-epitaxy dsa process. In *SPIE Proceedings Vol. 9053, March, 2014*.